AGU PUBLICATIONS

JGR

Journal of Geophysical Research: Solid Earth

RESEARCH ARTICLE
10.1002/2015JB011994

Key Points:
- Particles evolve morphologically during transport
- Fractal dimension decreases, whereas their circularity increases with distance
- Dynamic disintegration and particle interactions allow the flow mobility

Supporting Information:
- Text S1 and Figures S1–S3

Correspondence to:
H. Perinotto,
h.perinotto@epoc.u-bordeaux1.fr;
helene.perinotto@gmail.com

Citation:
Perinotto, H., J.-L. Schneider, P. Bachèlery, F.-X. Le Bourdonnec, V. Famin, and L. Michon (2015), The extreme mobility of debris avalanches: A new model of transport mechanism, *J. Geophys. Res. Solid Earth*, *120*, doi:10.1002/2015JB011994.

Received 7 MAR 2015
Accepted 8 NOV 2015
Accepted article online 18 NOV 2015

©2015. American Geophysical Union. All Rights Reserved.

The extreme mobility of debris avalanches: A new model of transport mechanism

Hélène Perinotto[1], Jean-Luc Schneider[1], Patrick Bachèlery[2], François-Xavier Le Bourdonnec[3], Vincent Famin[4], and Laurent Michon[4]

[1]Université de Bordeaux, UMR-CNRS 5805 EPOC, OASU, Allée Geoffroy Saint-Hilaire, Pessac, France, [2]Université Blaise Pascal, UMR-CNRS 6524-IRD163, Laboratoire Magmas et Volcans, OPGC, Clermont-Ferrand, France, [3]Université Bordeaux Montaigne, UMR-CNRS 5060 Centre de Recherche en Physique Appliquée à l'Archéologie (CRP2A), Maison de l'Archéologie, Esplanade des Antilles, Pessac, France, [4]Laboratoire Géosciences Réunion, Université de La Réunion, Institut de Physique du Globe de Paris, Sorbonne Paris-Cité, UMR 7154 CNRS, Saint-Denis, France

Abstract Large rockslide-debris avalanches, resulting from flank collapses that shape volcanoes and mountains on Earth and other object of the solar system, are rapid and dangerous gravity-driven granular flows that travel abnormal distances. During the last 50 years, numerous physical models have been put forward to explain their extreme mobility. The principal models are based on fluidization, lubrication, or dynamic disintegration. However, these processes remain poorly constrained. To identify precisely the transport mechanisms during debris avalanches, we examined morphometric (fractal dimension and circularity), grain size, and exoscopic characteristics of the various types of particles (clasts and matrix) from volcanic debris avalanche deposits of La Réunion Island (Indian Ocean). From these data we demonstrate for the first time that syn-transport dynamic disintegration continuously operates with the increasing runout distance from the source down to a grinding limit of 500 μm. Below this limit, the particle size reduction exclusively results from their attrition by frictional interactions. Consequently, the exceptional mobility of debris avalanches may be explained by the combined effect of elastic energy release during the dynamic disintegration of the larger clasts and frictional reduction within the matrix due to interactions between the finer particles.

1. Introduction

Debris avalanches are large-volume ($>10^6$ m^3) and high-speed mass movements that affect the flanks of mountainous and volcanic edifices on Earth and other objects of the solar system, for instance, the Moon, Mars, Venus, or Iapetus. They locally constitute an important natural hazard on Earth. They are characterized by an extreme mobility quantified by the apparent coefficient of friction defined as $\tan \alpha = H/L$, where H and L are the vertical and horizontal travel distances, respectively, between the crown and top [*Heim*, 1932; *Hsü*, 1978]. However, more recently, *Lucas et al.* [2014] propose an empirical relation, $\mu = (1/V)^{-0.0774}$, to calculate the mean effective friction from the avalanche volume.

Currently, the mechanisms involved in the extreme mobility remain poorly constrained for the geological community [*Shalle*, 1991; *Shaller and Smith-Shaller*, 1996; *Legros*, 2002; *Pollet and Schneider*, 2004]. The absence of a consensual explanation to the extreme mobility of the debris avalanches essentially stems in the difficulty of reconciling theoretical concepts with field observations regarding the internal organization of the deposits and the textural evolution of transported particles. There are many theoretical models for the extreme mobility of debris avalanche. *Hungr* [1990], *Davies et al.* [1999], and *Legros* [2002] present an exhaustive inventory. Since the 1960s these various hypotheses are based on the large-scale architecture of the deposits, theoretical approaches, and internal structural studies [*Hungr*, 2006; *Strom*, 2006; *Weidinger et al.*, 2014]. Some have been tested using numerical modeling by discrete element simulation [*Campbell*, 1989] or continuum models of granular flows [*Le Friant et al.*, 2003; *Lucas et al.*, 2014] as well as physical and analogue modeling [*Andrade and van Wyk de Vries*, 2010]. Overall, two main categories of models seem to rise from these efforts. On the one hand, mechanisms involving fluidization reduce the internal friction throughout the rock mass [*Rochet*, 1987] by incorporation of fluid as water [*Crandell et al.*, 1984], air [*Kent*, 1966], fine-grained matrix itself [*Hsü*, 1975, 1978], or release of acoustic waves [*Melosh*, 1987; *Collins and Melosh*, 2003]. On another hand, mechanisms involving lubrication reduce internal friction only in the basal part of the flow. They are based on the presence of an air cushion [*Shreve*, 1968; *Fahnestock*, 1978], water-saturated basal layer

[*Johnson*, 1978; *Voight and Sousa*, 1994], molten basal layer [*Erismann*, 1979; *De Blasio and Elverhøi*, 2008], or sliding sediment layer beneath the flow [*Watson and Wright*, 1967].

More recently, the concept of dynamic disintegration [*Schneider and Fisher*, 1998; *Davies and McSaveney*, 2006] has been proposed. It implies a fragmentation of the rock particles during the avalanche transport and induces both a clast size reduction by interparticle collisions and subsequent breakage with continuous energy release [*Linkov*, 1996; *Irme*, 2012] that could maintain the dilatancy of the granular mass and contribute to the extreme mobility. However, these various hypotheses suffer from the lack of a mass rock state quantification during the debris avalanche and require more detailed investigation to be identified as a realistic process.

The debris avalanche deposits of La Réunion Island (Indian Ocean) provide exceptional opportunities to observe the evolution of the particles throughout transport, because the deposits are accessible from the proximal to the distal parts. Our investigations are based on previous studies which have examined the characteristics of the particle for several debris avalanche deposits: Taranaki [*Ui et al.*, 1986], Mount St. Helens [*Komorowski et al.*, 1991], or Parinacota [*Clavero et al.*, 2002]. Thus, our approach consists of combining field studies, grain size, exoscopic, and new morphometric measurements using fractal dimension and circularity indicators based on various particle sizes. Our results bring new insights on processes which contribute to the extreme mobility of debris avalanches.

2. Geological Setting, Terminology, and Methods

2.1. Debris Avalanches of La Réunion Island

The building of large volcanic edifices, as La Réunion Island, involves a succession of phases of construction with the accumulation of lava flows and phases of destruction by massive flank landslides resulting from gravity instabilities. These large-scale landslides are the most important and efficient mass-wasting process on volcanoes. The largest debris avalanches have been observed on volcanic oceanic islands. The debris avalanche deposits of La Réunion Island result from the successive collapses of the Piton de Neiges volcano [*Bachèlery et al.*, 2003; *Bret et al.*, 2003], where they are found both in the inner part of the Piton des Neiges (Cirque de Mafate, Cirque de Salazie, and Cirque de Cilaos) and also near the shoreline.

We have investigated the debris avalanche deposits on the flanks of the Piton des Neiges volcano on La Réunion Island, at 10 sites (Figure 1) from the source scarp on the volcano (proximal zone) to the sea (distal zone). The average volume of each debris avalanche depositional unit is on the order of 1 km^3 [*Arnaud*, 2005; *Oehler*, 2005; *Lacquement and Nehlig*, 2008]. The topographic data indicate that the H/L ratio ($H = 3069$ m; $L = 25$ km) is around 0.13 and suggest that the debris avalanches were highly mobile. Applying the *Lucas et al.* [2014] empirical relation for effective friction (μ) to La Réunion debris avalanches, and considering a mean $V \sim 1$ km^3 for each debris avalanche unit, $\mu = 0.2$ confirms the high mobility of the debris avalanches.

Debris avalanche deposits are composed of fragments of aphyric and olivine basalts with minor quartz grains from hydrothermal veins. This compositional consistency argues for a single common volcanic source for all the avalanches. At all sites, particles forming the breccia deposits are highly fragmented with various sizes, up to a metric scale (polydisperse granular mass). Absence of fluid escape structures and strong particle packing argues within the deposits for very minor fluid presence or incorporation within the moving avalanches. Following Glicken's nomenclature [*Glicken*, 1991], the debris avalanche deposits contain large broken rock blocks with a jigsaw fit [*Ui et al.*, 1986; *Glicken*, 1991; *Shaller*, 1991, and references therein], the jigsaw blocks, embedded in a finer-grained matrix composed of apparently unbroken clasts, the individual clasts (Figure 2a). The jigsaw blocks are pieces of fragmented rocks that remain coherent without dispersion within the matrix despite their dense penetrative crack network [*Pollet and Schneider*, 2004]. The origin of the jigsaw fracturing remains poorly understood as some authors propose that the fractures of the transported rocks could predate the debris avalanche event [*Ui et al.*, 1986]. The general characteristics of the deposits at each site were studied through field observations, completed by morphometric measurements and textural scanning electron microscope (SEM) observations on particles, and grain size analyses.

2.2. Morphometric Methods

The morphometric analysis was based on digital images of a total of 5000 particle outlines of (1) jigsaw blocks and (2) individual clasts (Figure 2a), in the 5 mm–500 mm and 50 mm–80 μm grain size ranges, respectively.

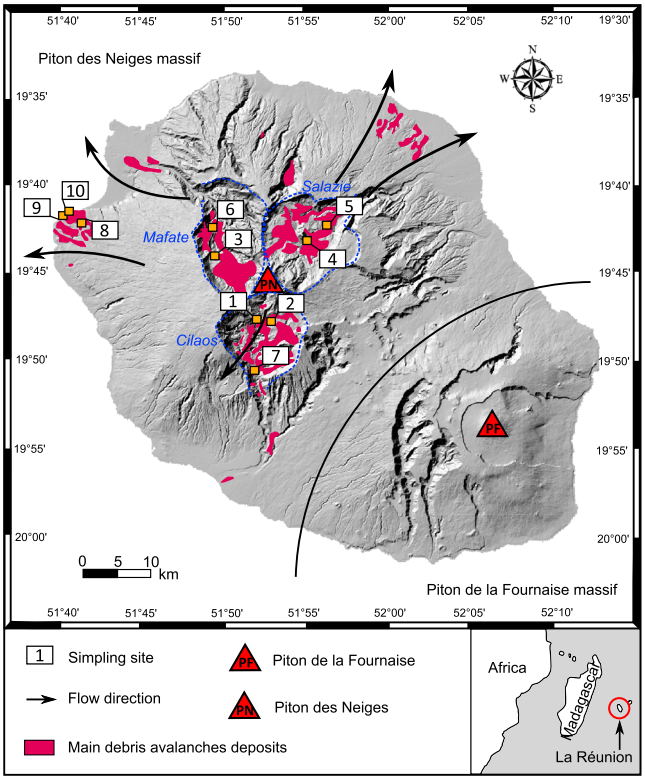

Figure 1. The map of La Reunion Island and location of the study area. Location of the debris avalanche deposits of the Piton des Neiges massif with main flow directions (arrows) and of the studied sites.

Analyzed particles were sampled in the core areas of the outcrop, except for site 10 where the particles were sampled at the base of the deposit. Our morphometric analyses include the simultaneous measurement of two shape parameters: the fractal dimension (FD) noted and the circularity (CIR) noted.

The fractal dimension [*Mandelbrot*, 1967; *Orford and Whalley*, 1987; *Turcotte*, 1992] provides information on the complexity of the particle's roughness (Text S1 in the Supporting Information). Values range between 1 and 2; the higher the value, the more complex the shape (Figure S1a in the supporting information). The concept of fractal dimension [*Allen et al.*, 1995] derives from the assumption that a stable linear relationship appears when the logarithm of the perimeter estimate (N) of an irregular particle outline is plotted against the logarithm of the step length ($1/\varepsilon$). Decrease in step length results in an increase of the perimeter by a constant value for particles whose morphological variations are the same at all measurement scales. The fractal dimension (FD) equals the slope coefficient of the best fitting linear regression of the plot (Figure S1a). Here we have used the box-counting method with the public domain Java-based image processing software package ImageJ® [*Rasband*, 2007] and with the FracLac® plug-in [*Karperien*, 2007] to compute the FD values (Figure S1b in the supporting information).

Circularity (CIR) [*Blott and Pye*, 2008] noted quantifies how the shape of the particle approaches that of a circle. Values range from 0 to 1, increasing as particles approach a circular shape. Particle outlines were scanned with a high-resolution scanner (2400 × 4800 dpi). CIR and FD measurements were based on binary 8-bit gamma-corrected particle pictures. Circularity values were also calculated with ImageJ® (Figure S2 in the supporting information).

2.3. Grain Size Distributions

Grain size distributions were determined exclusively for the fine-grained matrix (8 cm–63 μm grain size range) at each site to identify lateral evolution within the avalanche unit. Grain size distributions were measured on the >63 μm fraction by dry sieving. Each fraction was weighted and the number of particles calculated considering the mean density of the particles. Studied samples were collected at the 10 outcrops from the inner parts of the deposits to avoid the effects of more intense crushing occurring at the base.

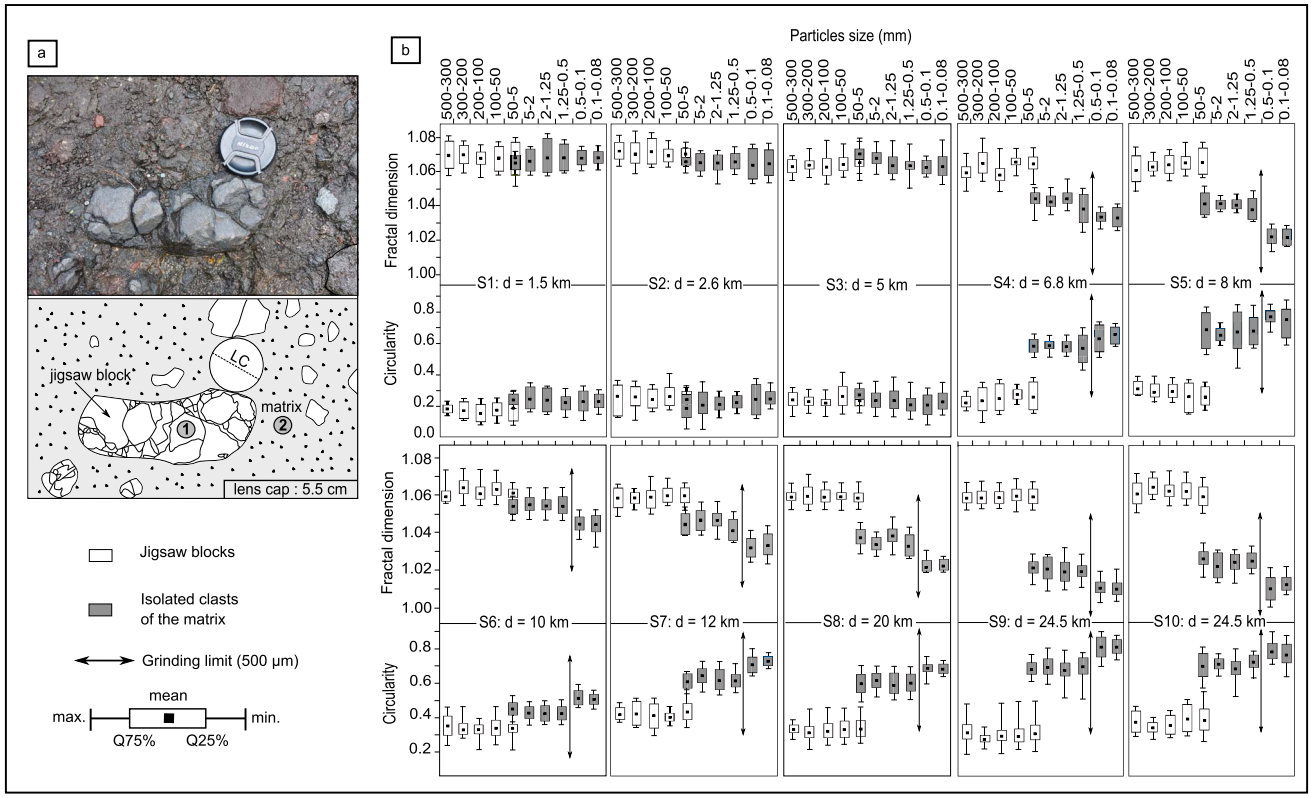

Figure 2. Results of the morphometric and grain size analyses. (a) Photographs of a typical jigsaw block and isolated clast present within the fine-grained matrix of the debris avalanche deposits. (b) Box plot data of the morphometric data (FD and CIR values) for the four studied sites along the proximal-distal transect. Jigsaw blocks do not show any variation of the FD and CIR values, whereas a morphological syn-transport evolution is clearly identified for the isolated clasts. Note the changes of the morphological evolution of the isolated clasts below the grinding limit (<500 µm) for sites 4 to 10.

2.4. Exoscopic Method

Exoscopic observations were made using the secondary electron imaging mode of the JEOL JSM-6460LV SEM. Prior to microscopic examination, the clay mineral coating of the particles were removed by ultrasonic and chemical cleaning following a protocol modified from *Komorowski et al*. [1991]. Particles were cleaned with a 5 min long ultrasonic treatment and put in a shaking hydrochloric acid (HCl 10%) bath for 7 min. They were subsequently rinsed one time with acetone and then rinsed again in pure water. Rinsed particles were placed in a 70% hydrogen peroxide solution for 12 h and rinsed with pure water. Finally, samples were dried at 50°C during 12 h.

3. Results

The morphometric values are presented in Figure 2b. Each box is the synthesis of 50 values of FD or CIR. CIR and FD values of jigsaw blocks are presented in grey boxes, and CIR and FD values of individual clasts are presented in white boxes. The mean FD values for the jigsaw blocks (1.066) do not display significant variability from proximal to distal sites. They are significantly lower for the individual clasts (1.043) and progressively decrease (1.09 > range of maximal variability >1.005) from proximal sites (sites 1 to 3) to distal sites (sites 8 to 10). The mean CIR (Figure 2b) of jigsaw blocks remain relatively constant (0.263), whereas they clearly increase for the individual clasts (0.489) in conjunction with distance from the source. FD and CIR values for both the jigsaw blocks and individual clasts are similar at the most proximal sampling locations (sites 1 to 3) but increasingly deviate from each other toward the more distal sites. Finally, except for sites 1, 2, and 3, both FD and CIR mean values of individual clasts are lower for particles with grain sizes below 500 µm.

A net change of grain size distributions is highlighted for the deposits at all sites (Figure S3 in the supporting information). Coarse particle (>500 µm) content is more abundant in proximal areas (sites 1 to 3), while the

Table 1. Percentage of Particles >500 μm and <500 μm for Each Studied Site[a]

Site	Supposed Distance From the Source	Clast < 500 μm (Percent of Total)	Clast > 500 μm (Percent of Total)
S1	1.5	87.31	12.72
S2	2.6	86.99	13.06
S3	5	86.37	13.73
S4	6.8	90.04	10.04
S5	8	88.36	11.71
S6	10	87.62	12.38
S7	12	89.69	10.40
S8	20	93.40	6.68
S9	24.5	93.49	6.51
S10	24.5	94.27	5.76

[a]The supposed distances from source give an approximate the value of travelled distance.

fine particles are clearly predominant in distal locations (sites 8 to 10). The proportion of particles >500 μm decreases with increasing runout distance (Table 1).

Moreover, SEM observations reveal a significant change in particle morphology around the 500 μm size. Particles >500 μm display microcracks that are similar to cracks observed in megablocks at the outcrop scale (Figures 3a–3j). The microcracks are sharp and deep without preferential shapes. The cracks of the particles typically show a three-dimensional jigsaw-fit texture with neither open spaces nor apparent relative displacement [*Davies and McSaveney*, 2009]. On the contrary, particles <500 μm do not exhibit any microcracks, except at sites

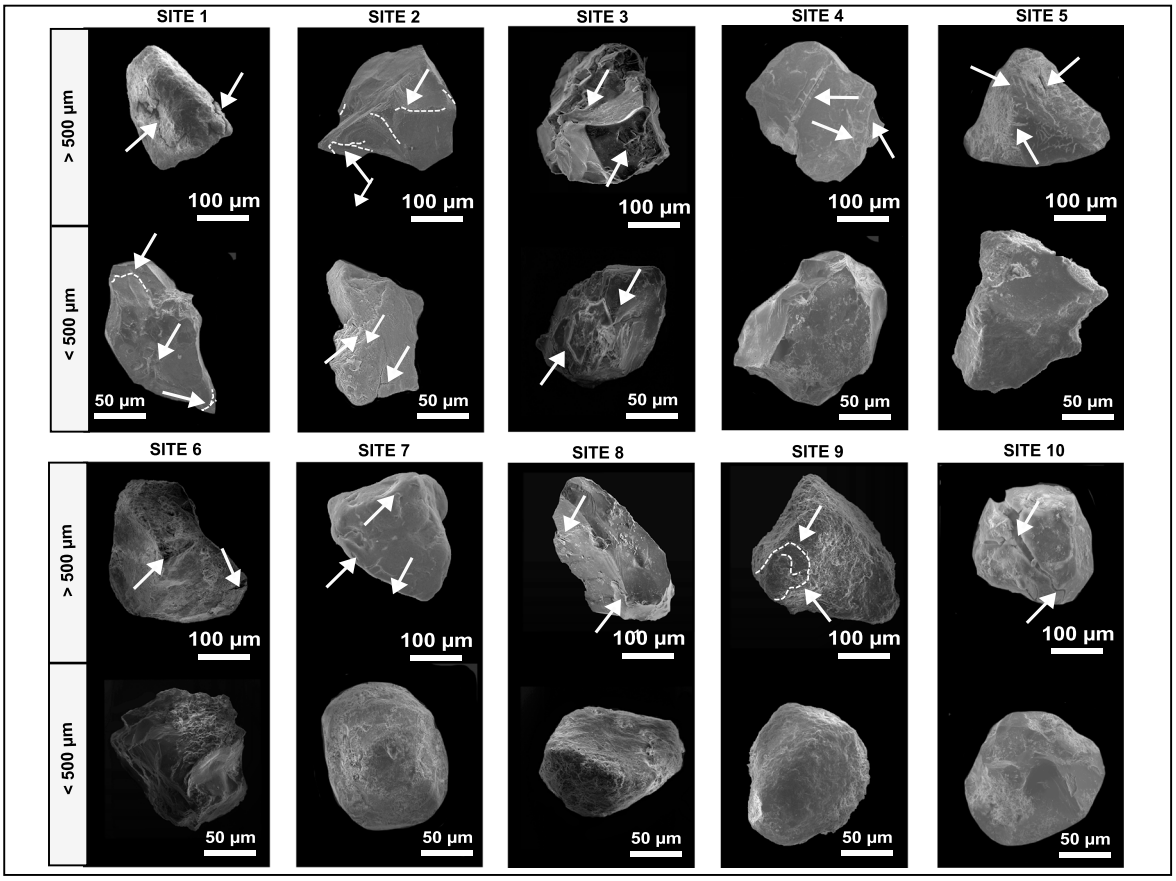

Figure 3. SEM photographs of particles from the matrix at all sites for grain sizes larger than and smaller than 500 μm. At sites 1, 2, and 3 particles from both grain size fractions display fresh cracks and broken surfaces (with arrows) indicating effective dynamic disintegration in the proximal and confined parts of the flow. For sites 4 to 10 cracks are observed exclusively on particles >500 μm (white arrows), whereas the finer particles have subrounded shapes and abraded edges.

1, 2, and 3 where they affect the lithic particles whatever their size (Figures 3k–3m). These observations are similar regardless of particle composition (feldspar and olivine crystals and sideromelane). Some observed irregularities, which cannot be considered as microcracks, correspond to abraded older notches. In the distal parts of the deposits more rounded particles $<500\ \mu m$ indicate strong abrasion during their transport within the matrix.

4. Interpretations and Discussion

We interpret the constant shape parameter values of the jigsaw blocks as a signature of dynamic disintegration that occurs continuously during transport and to the absence of significant subsequent abrasion of newly fragmented blocks (stabilities of FD and CIR values). As particles constituting jigsaw blocks remain packed together, the dynamic disintegration must have occurred uphill very close to the sampling location and just prior to the debris avalanche deposit. Thus, the elements of jigsaw blocks have not undergone any further textural maturation. Furthermore, the constant FD values at all sites indicate a common fracturing process for all the jigsaw blocks irrespective of their composition. Conversely, the progressive evolution with the distance of the CIR values of individual clasts reflects their textural maturation by abrasion during the transport after their formation by fracturing and further incorporation in the matrix. Concurrently, the progressive decrease of their FD values demonstrates their increasingly smooth character. A progressive grain size reduction occurs during the entire transport phase of the avalanche. It results in an increasing proportion matrix to blocks with distance in response to progressive dynamic disintegration of an increasing number of smaller particles.

Our most important discovery is the recognition of the grinding limit. The grinding limit is defined as the lower grain size for particles generated by dynamic disintegration in industrial grinders [*Boldyrev et al.*, 1996; *Cho et al.*, 1996]. The kinetics of particle breakage and the grinding limit depend on material properties as well as on process parameters influencing the stress intensity [*Knieke et al.*, 2009]. Here the grinding at $500\ \mu m$ is underlined by significant changes, below this limit, in FD and CIR values from sites 4 to 10. Below $500\ \mu m$, the dynamic disintegration does not operate further as suggested by a more mature texture of the finer particles. SEM observations confirm the existence of this limit, as particles smaller than $500\ \mu m$ never display any cracks for sites 4 to 10. In contrast, at sites 1 to 3, the finer particles ($<500\ \mu m$) are microfractured.

From these observations, we postulate that the initial kinetic energy of the avalanche, in conjunction with lithostatic pressure variations (loading and unloading of the granular mass above the fragmenting particles) and topographic confinement within the valleys walls, favors an intense syn-transport fragmentation and crushing near the source of the debris avalanche. More distally, as the avalanche mass spreads out and thins over a more open topographic surface, the confinement becomes inefficient and reduces dynamic disintegration of finer particles. Indeed, below the grinding limit, the inertia of the finer particles is too low to allow crushing during interparticle collisions. For these reasons, the grinding limit ($500\ \mu m$) is 10^2 to 10^4 times higher than for natural and experimental particle breakage in fault gouges that develop in more confined conditions [*Keulen et al.*, 2007]. The evidence of decrease of the confinement is highlighted by the spacing between the clasts in the jigsaw blocks. It has been measured in jigsaw blocks for each study site. The measurements were made using image analysis parameters of the software ImageJ® in comparing surface of jigsaw block with (surface S2) and without (surface S1) spaces (Figure 4a). It appears that the dispersive inflation of the jigsaw blocks after fracturing is more efficient in the distal stages of movement, increasing from approximately 10 to 20% in the proximal stages of the flow to 50 to 65% in the distal stages (Figures 4b–4d). We must note that the sample collected at site 10 was obtained from the base of the debris avalanche where the spaces are smaller.

These observations have important consequences on our understanding of the mechanisms operating during the transport of a debris avalanche. First, the dynamic disintegration by means of interparticle collisions, that leads to fracturing by impact loading [*Tavares and King*, 1998] and shearing within the granular mass, is driven by kinetic energy input during the initial acceleration of the mobile granular matter. After fracturing, inflation affects the jigsaw clasts and the progressive dispersion of the subparticles within the matrix suggests some degree of dispersion of the granular flow. The dynamic disintegration occurs continuously for larger particles ($>500\ \mu m$) throughout the transport, as long as the confinement of the debris avalanche remains sufficient to maintain an effective frictional stress and subsequent collisional fracturing. The elastic energy released during particle fragmentation events [*Liu et al.*, 2005], coupled with vibrations inducing by the moving mass, may serve to maintain the dilatancy necessary to keep the granular mass mobile [*Melosh*, 1979, 1987; *Collins and Melosh*, 2003].

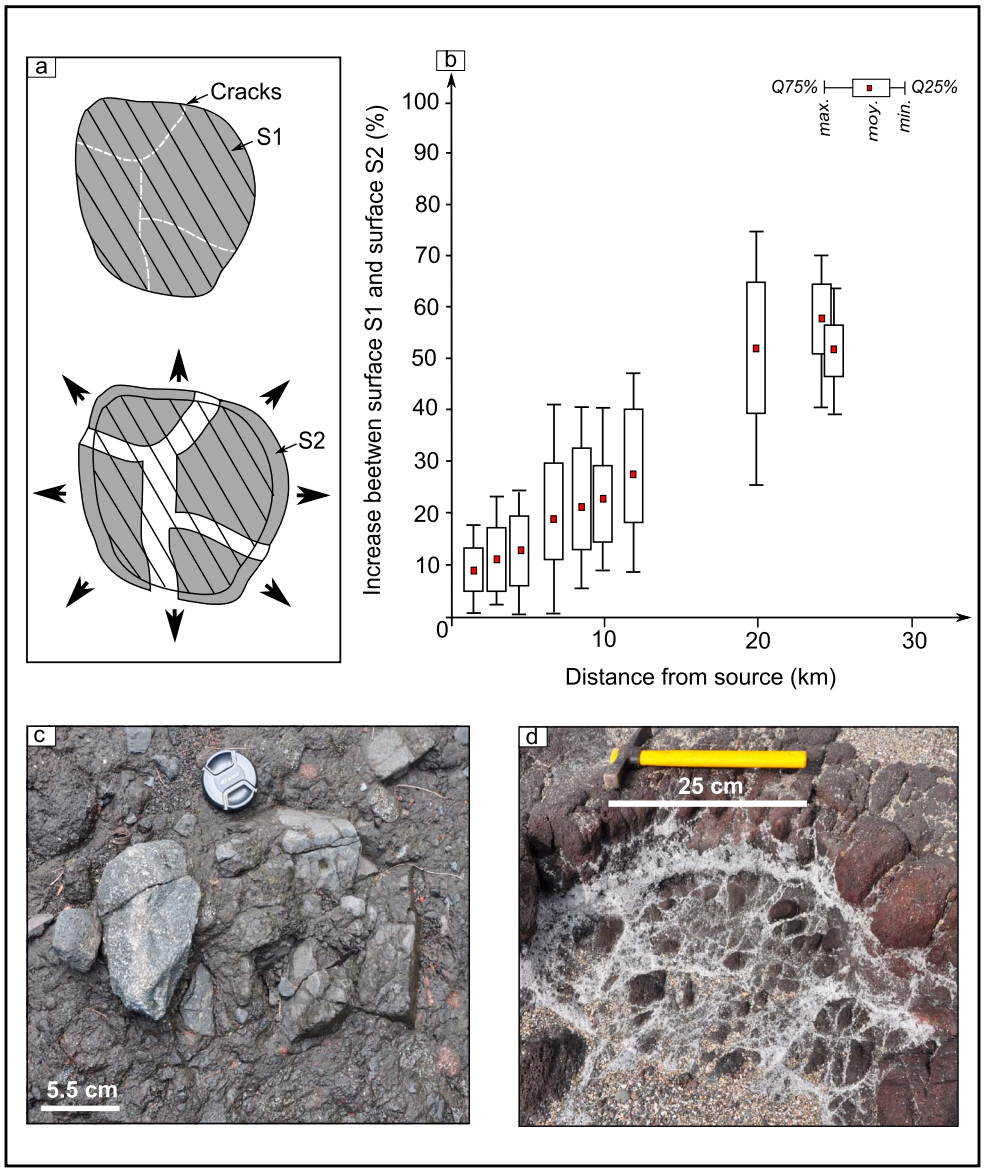

Figure 4. Evidence of dilatancy in the jigsaw block. (a) S1 shows the initial area of the block and S2 the area after dynamic disintegration. (b) Increase of the jigsaw block area after dynamic disintegration related to transport distance. (c) Jigsaw block in the very proximal part of the debris avalanche deposit. (d) Jigsaw block in the distal part of the debris avalanche deposit.

Second, it appears that dynamic disintegration cannot operate on particles $<500\ \mu m$, except in very proximal areas under efficient confinement conditions, as the kinetic energy of these finer particles is too low to lead to effective collisional crushing of finer particles. Third, fragmented particles that escape further crushing are then smoothed and rounded by frictional abrasion and their size is subsequently reduced. Both dynamic disintegration and abrasion of fine particles are also indicated by the evolution of grain size distributions of the matrix in which the proportion of the finer fraction ($<500\ \mu m$) significantly increases with the transport distance. The presence of this fine-grained matrix reduces the collision rate between coarser particles and partially inhibits the dynamic disintegration in distal parts of the debris avalanche. We consider however that the $<500\ \mu m$ fraction, below the identified grinding limit, behaves as an interstitial granular fluid of rounded particles that facilitates debris avalanche motion. Moreover, as suggested in previous studies [*Bagnold*, 1954; *Hsü*, 1975], by flowing and interacting between the larger particles, this fine-grained material (= interstitial fluid) could locally reduce the effective normal pressure on coarse grains and, consequently, diminish bulk frictional resistance, sustain dispersion, and fluidize the granular mass (Figure 5).

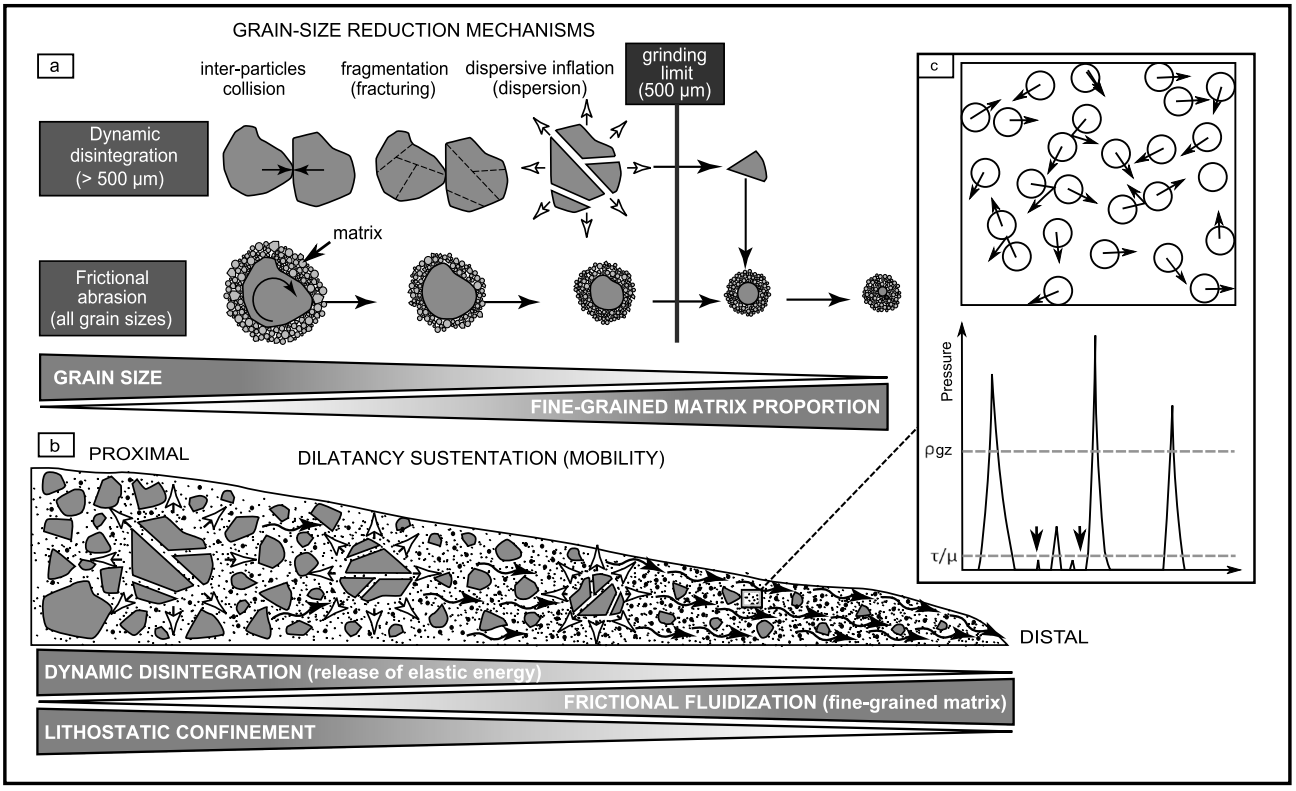

Figure 5. Schematic models illustrating particle size, shape evolution, and transport mechanisms during debris avalanche motion. (a) The successive dynamic disintegration steps are achieved by collisional loading on particles down to a 500 μm diameter (grinding limit). Fragmented particles are disseminated within the matrix by dispersive inflation. Frictional abrasion affects all particles whatever their size. (b) The dilatancy of the granular mass within the debris avalanche is favored by dynamic disintegration and the subsequent release of elastic energy, as well as by frictional fluidization of the fine-grained matrix. Both processes act simultaneously, but progressively decrease and increase, respectively, during the transport of the debris avalanche. (c) Interactions between the particles in the fine-grained matrix [from *Melosh*, 1987] which locally decrease the effective normal pressure in the rock mass.

Our results herein concern mainly the inner parts of the granular mass column, but our observations at site 10 (the base of a deposit) show that the particles are more mature (higher rounding and smoothness), whereas some studies on debris avalanches in other places suggest a more intense crushing within the sole of debris avalanche deposits [*Robinson et al.*, 2014]. In the case of La Réunion Island, we assume that the spreading of the granular mass in the last stages of the flow [*Bret et al.*, 2003; *Perinotto*, 2014] results of a substantial loose of topographic confinement with subsequent decrease of the thickness of the flow and resulting lithostatic confinement.

5. Conclusions

New data from La Réunion Island debris avalanche deposits strongly suggest that two consecutive and complementary major processes, occurring over the transport phase, were clearly identified from morphometric, textural, and grain size data:

1. Dynamic disintegration affects larger particles and is effective in producing relatively low fine-grained matrix proportions down to a grinding limit (500 μm) during the whole transport phase.
2. Below the grinding limit, interparticle interactions by contact or collision decreases effective normal pressure by stress transmission. These interactions favor the dispersion of the granular mass and rounding of the particles.

These two general processes were already, but independently, proposed by previous authors to explain the long runout of debris avalanches. Our work suggests that these two processes can both act together during debris avalanche transport. The mechanisms that support our model contribute together to sustain the

dispersion of the main part of the granular flow and provide arguments to explain the extreme mobility of debris avalanches. Thus, the processes acting exclusively at the base of the flows may not solely explain this mobility. They do not necessitate the role of any interstitial fluid (other than pulverized rock) as a lubricating agent and consequently can be applied to other telluric objects of the solar system. This would be in agreement with *Lucas et al.* [2014] who found a general trend in the decrease of the effective friction whatever the location of the landslide or debris avalanche is (on Earth and other planets). These processes are clearly important in the behavior or rock avalanches and must be considered in future modeling of these hazardous gravity flows.

Acknowledgments
Field work was supported by the French *Institut National des Sciences de l'Univers —CNRS* (grant ST-CT3-Risks-2012). M. Chaput is acknowledged for her assistance during the field work. Reviewers are also acknowledged for their insightful comments and sound advice that improved this work. The data for this paper are available by contacting the corresponding author.

References

Allen, M., G. J. Brown, and N. J. Miles (1995), Measurement of boundary fractal dimensions: Review of current techniques, *Powder Technol.*, *84*(1), 1–14.
Andrade, S. D., and B. van Wyk de Vries (2010), Structural analysis if the early stages of catastrophic stratovolcano flank-collapse using analogue models, *Bull. Volcanol.*, *72*(7), 771–789.
Arnaud, N. (2005), Les processus de démantèlement des volcans. Le cas d'un volcan bouclier en milieu océanique: le Piton des Neiges (Ile de la Réunion), PhD thesis, Dep. of Geosc., Univ. of La Réunion, La Réunion, France.
Bachèlery, P., B. Robineau, M. Courteaud, and C. Savin (2003), Avalanches de débris sur le flanc occidental du volcan bouclier du Piton des Neiges (Réunion), *Bull. Soc. Geol. Fr.*, *174*, 125–140.
Bagnold, R. A. (1954), Experiments on a gravity free dispersion of large solid spheres in a Newtonian fluid under shear, *Proc. R. Soc. London*, *225*, 49–63.
Blott, S. J., and K. Pye (2008), Particle shape: A review and new methods of characterization and classification, *Sedimentology*, *55*(1), 31–63.
Boldyrev, V. V., S. V. Pavlov, and E. L. Goldberg (1996), Interrelation between fine grinding and mechanical activation, *Int. J. Mineral. Proc.*, *44–45*, 181–185.
Bret, L., Y. Fèvre, J.-L. Join, B. Robineau, and P. Bachèlery (2003), Deposits related to degradation processes on Piton des Neiges Volcano (Reunion Island): Overview and geological hazard, *J. Volcanol. Geotherm. Res.*, *123*, 25–41.
Campbell, C. S. (1989), Self-lubrication for long runout landslides, *J. Geol.*, *97*, 653–665.
Cho, H., M. A. Waters, and R. Hogg (1996), Investigation of the grind limit in stirred-media milling, *Int. J. Miner. Process.*, *44–45*, 607–615.
Clavero, J. E., R. S. J. Sparks, H. E. Huppert, and W. B. Dade (2002), Geological constraints on the emplacement mechanism of the Parinacota debris avalanche, northern Chile, *Bull. Volcanol.*, *64*, 40–54.
Collins, G. S., and H. J. Melosh (2003), Acoustic fluidization and the extraordinary mobility of sturzstroms, *J. Geophys. Res.*, *208*(B10), 2473, doi:10.1029/2003JB002465.
Crandell, D. R., C. D. Miller, H. Glicken, R. L. Christiansen, and C. G. Newhall (1984), Catastrophic debris avalanche from ancestral Mount Shasta volcano, California, *Geology*, *12*, 143–146.
Davies, T. R. H., and M. J. McSaveney (2006), Runout of rock avalanches and volcanic debris avalanche, in *Proceedings of the International Conference on Fast Slope Movements: Prediction and Prevention for Risk Mitigation*, vol. 2, edited by L. Picarelli, pp. 113–132, Naples.
Davies, T. R. H., M. J. McSaveney, and K. A. Hodgson (1999), A fragmentation spreading model for long-runout rock avalanches, *Can. Geotech. J.*, *36*, 1096–1110.
De Blasio, V. F., and A. Elverhøi (2008), A model for frictional melt production beneath large rock avalanches, *J. Geophys. Res.*, *113*, F02014, doi:10.1029/2007JF000867.
Erismann, T. H. (1979), Mechanisms of large landslides, *Rock Mech.*, *12*, 15–46.
Fahnestock, R. K. (1978), Little Tahoma Peak rockfalls and avalanches, Mount Rainier, Washington, USA, in *Rockslides and Avalanches: Natural Phenomena*, vol. 1, edited by B. Voight, pp. 181–196, Elsevier, Amsterdam.
Glicken, H. (1991), Sedimentary architecture of large volcanic-debris avalanche, in *Sedimentation in Volcanic Settings*, *SEPM Spec. Publ.*, vol. 45, edited by V. Fisher and G. A. Smith, pp. 99–106, SPEM, Tulsa.
Heim, A. (1932), *Bergsturz und Menschenleben*, 218 pp., Fretz und Wasmuth Verlag, Zürich, Switzerland.
Hsü, K. J. (1975), Catastrophic debris streams (sturzstroms) generated by rockfalls, *Geol. Soc. Am. Bull.*, *86*, 129–140.
Hsü, K. J. (1978), Albert Heim: Observations on landslides and relevance to modern interpretations, in *Natural Phenomena*, vol. 1, edited by B. Voight, pp. 70–93, Elsevier, Amsterdam.
Hungr, O. (1990), Mobility of rock avalanches, *Report of the National Research Institute of Earth Science and Disaster Prevention*, Japan, *46*, 11–20.
Hungr, O. (2006), Rock avalanche occurrence, process and modelling, in *Landslides from Massive Rock Slope Failure NATO Science Series*, vol. 4, edited by S. G. Evans et al., pp. 243–266, Springer, Netherlands.
Irme, B. (2012), *Micromechanical Analyses of Sturzstroms (Rock Avalanches) on Earth and Mars*, 172 pp., VDF Verlag, Zürich, Switzerland.
Johnson, B. (1978), Blackhawk landslide, California, USA, in *Natural Phenomena*, vol. 1, edited by B. Voight, pp. 481–504, Elsevier, Amsterdam.
Karperien, A. (2007), FracLac for ImageJ version 2.5a [computer program], Research Services Branch, Natl. Inst. of Health, Bethesda, Md.
Kent, P. E. (1966), The transport mechanism in catastrophic rock falls, *J. Geol.*, *74*, 79–83.
Keulen, N., R. Heilbronner, H. Stünitz, A.-M. Boullier, and H. Ito (2007), Grain size distributions of fault rocks: A comparison between experimentally and naturally deformed granitoids, *J. Struct. Geol.*, *29*, 1282–1300.
Knieke, C., M. Sommer, and W. Peukert (2009), Identifying the apparent and true grinding limit, *Powder Technol.*, *195*, 25–30.
Komorowski, J.-C., H. Glicken, and M. F. Sheridan (1991), Secondary electron imagery and hackly fracture surfaces in sand-size clasts from the 1980 Mount St. Helens debris-avalanche deposit: Implications for particle-particle interactions, *Geology*, *19*(3), 261–264.
Lacquement F., and P. Nehlig (2008), Notice des cartes géologiques des cirques du Piton des Neiges (île de La Réunion, France), Final rapport, *BRGM/RP-56730-FR*, 96 pp.
Le Friant, A., P. Heinrich, C. Deplus, and G. Boudon (2003), Numerical simulation of the last flank-collapse event of Montagne Pelée, Martinique, Lesser Antilles, *Geophys. Res. Lett.*, *30*(2), 1034, doi:10.1029/2002GL015903.
Legros, F. (2002), The mobility of long-runout landslides, *Eng. Geol.*, *63*, 301–331.
Linkov, A. M. (1996), Rockburst and the instability of rock masses, *Int. J. Rock Mech.*, *33*(7), 727–732.
Liu, H. Y., S. G. Kou, and P.-A. Lindqvist (2005), Numerical studies on the inter-particle breakage of a confined particle assembly in rock crushing, *Mech. Mater.*, *37*(9), 935–954.

Lucas, A., A. Mangeney, and J.-P. Ampuero (2014), Frictional velocity-weakening in landslides on Earth and on other planetary bodies, *Nat. Commun.*, *5*, 3417, doi:10.1038/ncomms447.
Mandelbrot, B. B. (1967), How long is the coast of Britain? Statistical self-similarity and fractal dimension, *Science*, *156*, 636–638.
Melosh, H. J. (1979), Acoustic fluidization: A new geologic process, *J. Geophys. Res.*, *84*, 7513–7520, doi:10.1029/JB084iB13p07513.
Melosh, H. J. (1987), The mechanism of large rock avalanches in debris flow/avalanches: Process, recognition, and mitigation, edited by J. E. Costa and G. F. Wieczorek, Geol. Soc. Am, *Rev. Eng. Geol.*, *7*, 41–50.
Oehler, J.-F. (2005), Les déstabilisations de flanc des volcans de l'île de La Réunion (Océan Indien): Mise en évidence, implications et origines, MS thesis, Dep. of Geol., Univ. Blaise Pascal, Clermont-Ferrand, France.
Orford, J. D., and W. B. Whalley (1987), The quantitative description of highly irregular sedimentary particles: The use of fractal dimension, in *Clastic Particles*, edited by J. R. Marshall, pp. 267–289, Van Nostrand Reinhold Company, New York.
Perinotto, H. (2014), Dynamique de mise en place des avalanches de debris sur les flancs aériens des volcans insulaires, le cas de La Réunion, PhD thesis, Dep. of Geol., Univ. of Bordeaux, Pessac, France.
Pollet, N., and J.-L. Schneider (2004), Dynamic disintegration processes accompanying transport of the Holocene Flims sturzstrom (Swiss Alps), *Earth Planet. Sci. Lett.*, *221*, 433–448.
Rasband, W. S. (2007), *ImageJ*, U.S. Natl. Inst. of Health, Bethesda, Md.
Robinson, T. R., T. R. H. Davies, N. V. Reznichenko, and G. P. De Pascale (2014), The extremely long-runout Komansu rock avalanche in the Trans Altai Range, Pamir Mountains, southern Kyrgyzstan, *Landslides*, doi:10.1007/s10346-014-0492-y.
Rochet, L. (1987), Application des modèles numériques de propagation à l'étude des éboulements rocheux, *Bull. Liaison Lab. Ponts Chaussées*, *150*, 84–95.
Schneider, J.-L., and R. V. Fisher (1998), Transport and emplacement mechanisms of large volcanic debris avalanches: Evidence from the northwest sector of Cantal Volcano (France), *J. Volcanol. Geothem. Res.*, *83*, 141–165.
Shaller, P. J. (1991), Analysis and implications of large Martians and terrestrial landslides, PhD thesis, Calif. Inst. of Technol., Pasadena, Calif., 586 pp.
Shaller, P. J., and A. Smith-Shaller (1996), Review of proposed mechanisms for sturzstroms (long runout landslides), in *Sturzstroms and Detachment Faults, Anbza-Boreego Desert State Park, California*, edited by P. L. Abott and D. C. Semour, pp. 195–202, South Coast Geol. Soc., Santa Ana, Calif.
Shreve, R. L. (1968), The Blackhawk landslide, *Geol. Soc. Am. Spec. Pap.*, *108*, 1–47.
Strom, A. (2006), Morphology and internal structure of rockslides and rock avalanches: Ground and constraints for their modelling, in *Landslides from Massive Rock Slope Failure NATO Science Ser.*, vol. 4, edited by S. G. Evans et al., pp. 305–326, Springer, Netherlands.
Tavares, L. M., and R. P. King (1998), Single-particle fracture under impact loading, *Int. J. Miner. Process.*, *54*, 1–28.
Turcotte, D. L. (1992), *Fractals and Chaos in Geology and Geophysics*, 2nd ed., Cambridge Univ. Press, Cambridge.
Ui, T., S. Kawachi, and V. E. Neall (1986), Fragmentation of debris avalanche material during flowage. Evidence from the Pungarehu Formation, Mount Egmont, New Zealand, *J. Volcanol. Geotherm. Res.*, *27*, 255–264.
Voight, B., and J. Sousa (1994), Lessons from Ontake-san: A comparative analysis of debris avalanche dynamics, *Eng. Geol.*, *38*, 261–297.
Watson, R. A., and H. E. Wright (1967), The Saidmarreh landslide, Iran, *Geol. Soc. Am. Spec. Pap.*, *123*, 115–139.
Weidinger, J. T., O. Korup, H. Munack, U. Altenberger, S. Dunning, G. Tippelet, and W. Lottermoser (2014), Giant rockslides from the inside, *Earth Planet. Sci. Lett.*, *389*, 62–73.